energies

MDPI

Article

Microstructure-Driven Hygrothermal Behavior of Mycelium-Based Composites for Bio-Based Insulation

Sina Motamedi [1], Daniel R. Rousse [1,*] and Geoffrey Promis [2]

[1] Research Group in Energy Technologies and Energy Efficiency (t3e), École de Technologie Supérieure (ÉTS), Université du Québec, Montreal, QC H3C 1K3, Canada; seyedsina.motamedi.1@ens.etsmtl.ca
[2] University of Picardie Jules Verne, Innovative Technologies Laboratory (LTI), 80025 Amiens Cedex, France; geoffrey.promis@u-picardie.fr
* Correspondence: daniel.rousse@etsmtl.ca; Tel.: +1-(514)-396-8462

Abstract: This study investigates the coupled hygrothermal behavior of mycelium-based composites (MBCs) as a function of their microstructural organization, governed by fungal species, substrate type, additive incorporation, and treatment method. Eleven composite formulations were selected and characterized using a multi-scale experimental approach, combining scanning electron microscopy, dynamic vapor sorption, vapor permeability tests, capillary uptake measurements, and transient thermal conductivity analysis. SEM analysis revealed that *Ganoderma lucidum* forms dense and interconnected hyphal networks, whereas *Trametes versicolor* generates looser, localized structures. These morphological differences directly influence water vapor transport and heat conduction. Additive-enriched composites exhibited up to 21.8% higher moisture uptake at 90% RH, while straw-based composites demonstrated higher capillary uptake and free water saturation (up to 704 kg/m^3), indicating enhanced moisture sensitivity. In contrast, hemp-based formulations with *Ganoderma lucidum* showed reduced sorption and vapor permeability due to limited pore interconnectivity. Thermal conductivity varied nonlinearly with temperature and moisture content. Fitting the experimental data with an exponential model revealed a moisture sensitivity coefficient thirty times lower for GHOP compared to VHOP, highlighting the stabilizing effect of a compact microstructure. The distinction between total and effective porosity emerged as a key factor in explaining discrepancies between apparent and functional moisture behavior. These findings demonstrate that hygric and thermal properties in MBCs are governed not by porosity alone, but by the geometry and connectivity of the internal fungal network. Optimizing these structural features enables fine control overheat and mass transfer, laying the groundwork for the development of high-performance, bio-based insulation materials.

Keywords: bio-based building materials; fungal insulation materials; hygrothermal behavior modeling; vapor permeability in mycelium-based insulation; thermal conductivity of porous materials; GAB sorption model; scanning electron microscopy (SEM) in biocomposites; *Ganoderma lucidum* vs. *Trametes versicolor*

Academic Editors: Árpád Nyers and Jozsef Nyers

Received: 20 April 2025
Revised: 17 May 2025
Accepted: 21 May 2025
Published: 30 May 2025

Citation: Motamedi, S.; Rousse, D.R.; Promis, G. Microstructure-Driven Hygrothermal Behavior of Mycelium-Based Composites for Bio-Based Insulation. *Energies* **2025**, *18*, 2864. https://doi.org/10.3390/en18112864

1. Introduction

The construction industry, contributing approximately 38% of global carbon emissions [1], faces mounting pressure to adopt sustainable materials that address both embodied and operational carbon. In Canada, commercial and institutional buildings account for 18% of total energy demand, with the residential sector adding 33% [2]. Embodied energy,

which is often overlooked, constitutes 10–30% of a building's carbon emissions [3–5], emphasizing the need to transition from zero-energy buildings (ZEB) to life-cycle zero-energy buildings (LCZEB) [6]. Mycelium-based composites (MBCs) are sustainable insulation alternatives produced through the colonization of agricultural by-products by fungal mycelium. Mycelium acts as a natural binder, replacing chemical binders such as lime, and offers sustainability benefits due to its low carbon footprint, biodegradability, and carbon sequestration ability during growth [7–9]. These qualities position MBCs as viable alternatives to energy-intensive insulation materials like expanded polystyrene (EPS).

Recent research has advanced MBC property understanding, yet hygrothermal studies remain limited. Elsacker et al. (2021) explored moisture uptake in extruded MBCs, showing resilience under different hygric conditions [10]. Koh et al. (2022) measured thermal conductivity (0.06–0.08 W/m·K) and moisture uptake in mycelium-based insulation composites, highlighting substrate influence in their physical properties [11]. Yang et al. (2021) reviewed MBC functionality, noting thermal insulation potential akin to EPS [12]. Gauvin et al. (2022) reported low thermal conductivity (0.05–0.07 W/m·K) and good moisture buffer capacity in MBCs as foam-like insulation [13]. Schultz et al. (2024) demonstrated thermal stability (0.06 W/m·K post-weathering) under simulated conditions [14]. Farrahnoor et al. (2024) improved water barrier properties of MBCs with beeswax coatings, aiding thermal performance [15]. Additionally, in terms of carbon emission, Alaux et al. (2023) and Stelzer et al. (2021) quantified environmental benefits, with the latter reporting a carbon footprint of 0.3–0.7 kg CO_2e/kg for MBC bricks [8,16].

Recent studies on mycelium-based composites (MBCs) leverage scanning electron microscopy (SEM) to elucidate how microstructural features govern hygrothermal performance. Haneef et al. (2017) utilized cryo-SEM to examine MBCs from *Ganoderma lucidum* and *Pleurotus ostreatus* grown on cellulose-based substrates, demonstrating that substrate-driven variations in hyphal morphology and composition, such as increased chitin content, directly enhance water absorption rates, a key hygrothermal property [17]. Gauvin et al. (2021) [13] reported that extended fungal growth forms a denser mycelium layer, improving water resistance and influencing thermal conductivity, with microstructural insights supported by SEM-based studies they reference, such as Elsacker et al. (2019) [18]. Yang et al. (2021) reviewed SEM analyses of species like *Trametes versicolor* and *Ganoderma lucidum*, linking species-specific structural variations, particularly porosity, to thermal insulation and moisture buffering capacity [12].

Despite recent advancements in the study of MBCs, significant research gaps remain, particularly regarding the correlation between their microstructure and comprehensive hygrothermal properties. The existing literature has predominantly focused on basic parameters such as thermal conductivity, moisture uptake, and mechanical strength, while more detailed hygrothermal characteristics, such as sorption isotherms, vapor permeability, and moisture buffer values, have been largely overlooked. Furthermore, the lack of an established link between microstructural features and hygrothermal performance hinders the optimization of MBCs for practical applications in sustainable building insulation.

To address these research gaps, this study systematically characterizes the microstructural and hygrothermal properties of MBCs, fabricated from hemp and straw substrates colonized by *Ganoderma lucidum* and *Trametes versicolor*. The study evaluates how variations in substrate–fungus combinations and fabrication parameters influence the microstructure of samples. Accordingly, this study entails the characterization of key insulation properties, including moisture adsorption, vapor permeability, water uptake and thermal conductivity. By integrating scanning electron microscopy (SEM) with hygrothermal analysis, the research seeks to establish a direct correlation between microstructural characteristics and

material performance, offering valuable insights into fungal–substrate interactions and optimizing MBC design for sustainable building insulation.

This paper is organized to present the investigation of MBCs as sustainable insulation materials. Section 2 outlines the materials and experimental methods alongside the governing equation used for the calculation of physical properties. It encompasses the fabrication of MBCs and the protocols for microstructural and hygrothermal characterization. Section 3 reports the findings, detailing microstructural analysis via scanning electron microscopy (SEM), alongside hygric and thermal property assessments. The discussions are included in this section alongside the presented results. Section 4 summarizes the key outcomes, their implications for sustainable building insulation and proposes directions for future research. To provide a comprehensive understanding of these effects, a detailed experimental approach is necessary to isolate the influence of fungal species, substrates, and processing conditions on microstructural and hygrothermal outcomes.

2. Material and Methods

This section presents the materials used and the procedures followed for fabricating and testing MBCs, allowing for the systematic characterization of their structural, hygric, and thermal behavior.

2.1. Materials Preparation

Tested MBCs were fabricated using two fungal species: *Ganoderma lucidum* and *Trametes versicolor* and two types of agricultural substrates, hemp shiv and wheat straw. Substrates were sourced locally, cleaned, and sieved to particle sizes between 2 mm and 10 mm to achieve consistent composite textures. Two organic nutritional additives, wheat bran and soybean meal, were utilized to enhance fungal colonization. Each composite mixture comprised substrate, fungal spawn, and additives in specific weight ratios detailed below. Three disinfection methods were examined: unpasteurized (ambient), pasteurized (80 °C for 60 min), and sterilized (121 °C, 15 psi for one hour), to evaluate their effect on fungal growth and composite properties.

Formulations followed these ratios:

- Substrate (hemp or straw): 50% dry mass;
- Fungal spawn: 33% dry mass;
- Nutritional additive (wheat bran or soybean meal): 17% dry mass (only for specific formulations indicated below);
- Water content adjusted to 233% of dry mass using distilled water.

The prepared mixtures were then inoculated for 7 days in plastic bags at controlled conditions (temperature: 26–28 °C, relative humidity: 65–75%) for 7–8 days. Inoculated samples were then placed into rectangular and cylindrical molds with dimensions adjusted for planned hygrothermal tests (R1: 35 × 35 × 162 mm^3; R2: 35 × 90 × 162 mm; R3: 500 × 500 × 30 mm^3; C1: Cylindrical D103, H30 mm; C2: Cylindrical D118, H30 mm). For each formulation in each test, three samples were fabricated to ensure the repeatability of the experimental results. The samples were then covered with plastic and incubated at the same controlled conditions for another 7–8 days. Samples were demolded and left for an additional 7 days of incubation for the edges of the samples to be fully colonized by mycelium. The process was then followed by drying process at 60 to 65 °C until mass stabilization, which is typically achieved within 48 to 96 h.

2.2. Sample Nomenclature

Sample naming conventions consistently follow substrate–fungus–additive–disinfection order:

- Fungus species: *Ganoderma lucidum* (G), *Trametes versicolor* (V);
- Substrate: Hemp (H), Straw (S);
- Additive: With additive (W), Without additive (O);
- Disinfection method: Unpasteurized (U), Pasteurized (P), Sterilized (S).

Thus, for instance, the sample "GHOP" denotes *Ganoderma lucidum* colonized on Hemp substrate, withOut additives, and Pasteurized. Using this mixture to systematically investigate the influence of compositional and processing variables on the hygrothermal performance of mycelium-based composites (MBCs), a total of 11 formulations were prepared. These formulations vary in terms of fungal species, substrate type, presence of additives, and processing treatments. This variety was designed to account for a realistic range of material conditions encountered in MBCs fabrication methods. The selection of specific formulations for each test was guided by the suitability of the sample for the target property being measured. For example, for microstructural analysis, two samples were chosen to highlight the differences resulting from the use of different fungal species; for thermal conductivity measurements, the most cohesive specimens with the lowest densities and highest porosity were selected; and for hygric tests, a representative subset was selected to encompass variation across all major fabrication parameters, supporting a more comprehensive interpretation of moisture-related behavior.

2.3. Microstructural Characterization

Scanning Electron Microscopy (SEM) was performed using selected representative samples (GHOP and VHOP) to qualitatively analyze fungal colonization, network density, substrate interaction, and internal morphology. Samples were prepared by slicing small segments ($1 \times 1 \times 5$ mm^3) from the center of cured composites, mounted on SEM stubs, and gold-coated for 120 s using sputter coating. Images were captured at magnifications ranging from 30× to 7000×, providing insights into microstructural differences associated with fungal species and substrates.

2.4. Hygric Characterization

Sorption isotherm analysis was performed using a Dynamic Vapor Sorption (DVS) device. The ProUmid DVS device, is manufactured by ProUmid GmbH & Co., KG, which is headquarters in Ulm, Baden-Württemberg, Germany. This device is used for these measurements offers a mass precision of 0.01 mg with an uncertainty of ±0.005% for moisture content, and controls relative humidity with a precision of ±0.1% and an uncertainty of ±1% to ±1.5%. The device was programmed to vary the relative humidity (RH) over the range of 0 to 90% RH in 10% humidity range steps. Sorption isotherms are characterized at five different temperatures to assess the temperature's influence on the adsorption behavior. Five samples are characterized including GHOP, GHOU, GHWU, GSWP, and VHOP (see Nomenclature for definitions).

The GAB model is employed to characterize the hygric behavior of the tested composites during adsorption. It enables the modeling of a material's hygroscopic behavior across the entire spectrum of relative humidity from 0% to 100%. The relationship between the moisture content (u) and the relative humidity (ϕ) based on this equation is as follows:

$$u(\phi) = \frac{w_m C K \phi}{(1 - K\phi)(1 - K\phi + CK\phi)}, \quad (1)$$

where w_m represents the moisture content associated with an adsorbed monolayer, while C and K are coefficients dependent on the molar heat of absorption and the latent heat of condensation, respectively.

The vapor permeability of the bio-composites was determined using the dry method, which involves creating a dry environment beneath the sample and subjecting the top to controlled environmental condition of 50% relative humidity in the climatic chamber. The successive mass variations in the last five measurements should be less than 5% of the difference in the initial and final moisture content of the sample. The diffusion coefficients for vapor transfer using the dry methods are calculated based on Equation (2) as a function of relative humidity or moisture content. The tested samples in the permeability test are VSOP, GSWP, and GHWU.

$$g_v = -\delta_p \nabla P_v = -\delta_p P_{v,sat} \nabla \phi = -D_{v,\varphi} \nabla \phi = -D_{v,w} \nabla w = -\frac{\delta_p P_{v,sat}}{\xi_\phi} \nabla w, \quad (2)$$

where g_v is the vapor flux, δ_p represents the water vapor permeability, and P_v denotes the partial vapor pressure, $P_{v,sat}$, corresponds to the saturation vapor pressure, while ϕ represents the relative humidity. The vapor diffusion coefficient as a function of relative humidity and moisture content are denoted by $D_{v,\varphi}$ and $D_{v,w}$, respectively. w indicates the moisture content, and ξ_ϕ is the slope of the sorption isotherm. Accordingly, the resistance factor is calculated as follows:

$$\delta_p = \frac{\delta}{\mu}, \quad (3)$$

where δ_p is the vapor permeability of the material, and μ is the water vapor diffusion resistance factor. By applying a capillary boundary condition, the capillary diffusion coefficient can be determined, representing the liquid moisture transport within the material at elevated moisture contents. The capillary coefficient will be calculated as a function of moisture content.

$$g_w = -D_{l,w}(w) \nabla w, \quad (4)$$

where g_w represents the liquid water flux and $D_{l,w}$ is the liquid water diffusivity. Alternatively, Künzel [19] established an approximation to define a liquid transport coefficient, as follows:

$$D_{ws} = 3.8 \times \left(\frac{A_c}{w_f}\right)^2 \times 1000^{\left(\frac{w}{w_f}-1\right)}, \quad (5)$$

$$D_{ws} = D_{l,w}, \quad (6)$$

where D_{ws} and $D_{l,w}$ both represent the liquid water diffusivity, with D_{ws} specifically referring to diffusivity under saturation conditions. A_c is absorption coefficient of water, w_f is the free water saturation, and w is the actual moisture content. By plotting mass per unit area against the square root of time, A_c is determined from the slope of the capillary sorption graphs. The principle of the test is to measure the mass evolution of samples that are in contact with water. This condition is achieved by placing the samples on a grid and immersing them to a depth of approximately 3 mm. The tested samples are of dimensions 38 × 31 × 100 mm^3. Three different samples from the mixtures of Straw and Hemp with *Ganoderma lucidum* (GSWP, GHOU, and GHOP) are tested. For each type of composite, three samples were prepared. The specimens are cut to eliminate the layer that was in contact with the mold. The samples are then dried in an oven at 70 °C, which is the maximum permissible temperature to prevent MBC decomposition, until the mass stabilizes. The lateral faces of the samples are isolated using cellophane and aluminum foil tape. At the beginning of the test, mass measurements were taken at 30 s intervals, followed by measurements at 1 min, 5 min, 10 min, 20 min, and 1 h. Before each measurement, the specimen is superficially drained and wiped.

The measurement of the free water saturation samples are measured through submerging cylindrical samples with the dimensions D90 mm and H25 mm. The samples

are initially placed in a sealed chamber and vacuumed for 2 h to remove the air trapped in the open pores of the material. The chamber is then filled with water and resealed, with samples submerged in the water. The same vacuum pump is used to ensure that the cavities of the samples are effectively filled with water. The weight is monitored hourly until the mass of the samples stabilizes. The weight of water adsorbed by the sample was measured in 0.1 g increments until the weight stabilized over three consecutive measurements. Three samples of each type of bio-composite were utilized. Free water saturation in Equation (7) indicates the open porosity of the material, while the maximum water content, denoted as w_{max}, reflects the filling of all cavities (open and closed) in the material, representing total porosity. Measuring the maximum water content is often impractical because closed porosity requires pycnometry tests, which involve crushing the material into powder, a challenging process due to the material's compressible nature and resistance to pulverization. Therefore, free water saturation substitutes this parameter in the equations. Additionally, as shown later in this paper, the majority of the material's porosity is open, so this assumption does not compromise the accuracy of the results. It is noteworthy that based on this study's findings, the majority of material porosity is open, thereby minimally affecting the results.

$$w_f = \rho_w \cdot n, \tag{7}$$

where w_f represents the free water saturation as previously discussed, ρ_w is the density of water, and n denotes the porosity of the material.

2.5. Thermal Characterization

Thermal conductivity and specific heat capacity are measured as the basic thermal properties. The Transient Plane Source (TPS) method is used for thermal characteristic measurements. The TPS device operates by employing a transient heat source to measure thermal conductivity. It consists of a sensor with a flat, thin, and round probe that is heated for a short duration. The temperature response of the material undergoing testing is then monitored, and the thermal conductivity is determined based on the rate at which heat is transferred through the sample. This method allows for quick and accurate measurements of thermal conductivity across a wide range of materials.

Using TPS, thermal conductivity is measured for three relative humidities (0, 50 and 80 percent) and three different temperatures (10 °C, 20 °C and 30 °C). The relative humidity and temperature conditions are adjusted by placing both the TPS device and the test sample inside a climatic chamber throughout the duration of the measurement. Four samples are characterized, including GHOP, GSWS, GSOS, and VHOS. Relative humidity causes fluctuations in material moisture content, thereby directly impacting thermal conductivity. Increasing temperature can partially increase pore diameters, thus directly affecting thermal conductivity. However, its primary influence indirectly occurs by changing saturation pressure as follows [20]:

$$p_v^{sat} = \exp\left[23.5771 - \frac{4042.9}{T - 37.58}\right], \tag{8}$$

where p_v^{sat} is the saturation vapor pressure, and T represents the temperature.

With a robust experimental protocol in place, the results derived from SEM analysis and hygrothermal testing now offer insights into the material's behavior and performance trends.

The extension of the testing procedures described is summarized in Table 1, which details the test types, number of replicates, sample formulations, and corresponding dimensions.

Table 1. Summary of sample types, formulations, and dimensions used.

Test Type	Number of Samples for Each Formulation	Sample Formulations	Sample Dimensions
Microstructural Characterization	3	VHOP, GHOP	1 × 1 × 5 (mm)
Sorption Isotherms (DVS)	3	GHOP, GHOU, GHWU, GSWP, VHOP	30 × 40 × 50 (mm)
Water Vapor Permeability	3	VSOP, GSWP, GHWU	Cylindrical D103, H30 (mm)
Water Absorption	3	GSWP, GHOU, GHOP	Cylindrical D103, H30 (mm)
Thermal Conductivity	3	GHOP, GSWS, GSOS, VHOS	Cylindrical D103, H30 (mm)

3. Results and Discussion

The following section presents and interprets the key findings from structural, hygric, and thermal characterization, linking them to the underlying material formulations and microstructural features.

3.1. Microstructural Characterization

This analysis aimed to examine the interaction between fungal mycelium and hemp substrate, the formation of hyphal networks, and the overall material morphology. Understanding these microstructural features is essential, as they directly influence the mechanical integrity, porosity, and interfacial bonding within the composite. The analysis focused on two selected samples: GHOP and VHOP.

By analyzing high- and low-magnification images, SEM provides insights into the extent of mycelial colonization, fiber–matrix adhesion, and the presence of microstructural voids or reinforcements. These observations help assess how fungal growth patterns contribute to the composite's structure, potentially impacting its mechanical and moisture-related properties. The following section presents the microstructural observations derived from SEM imaging.

Both mycelium species form a network of filamentous structures called hyphae (Figure 1). These networks exhibit similar morphology, consisting of numerous branches. Each filamentous hypha elongates outward, fusing with other growing filaments to form a large "fractal network" structure. According to A. Farrahnoor et al. [15], mycelium develops by consuming nutrients from substrates, decomposing organic matter, and converting it into compounds for its growth.

The interwoven structure of the hyphae indicates a dense network, suggesting effective substrate colonization, which is crucial for the formation of MBCs. According to Yang et al. [12], the elongated and thin appearance of the hyphae likely results from shrinkage during the drying process, as the hyphae lose water content. The observed filament diameters range from 1 to 3 μm for GHOP and approximately 1 μm for VHOP, aligning with the lower range of white mycelium filament dimensions (1–30 μm) reported by Yang et al. [12].

Based on the interaction between mycelium and substrate observed in the images, the multi-scale fiber effect between mycelium and granules might have influenced the composite's mechanical properties. This effect refers to how the mycelium's filamentous network (hyphae) intertwines with and binds the hemp granules at different scales. Such an interaction can enhance impact resistance, as demonstrated by J. Cai et al. [21]. The dense,

interconnected mycelial network likely strengthens bonding between granules, distributes stress more effectively, and improves energy dissipation upon impact, contributing to greater durability.

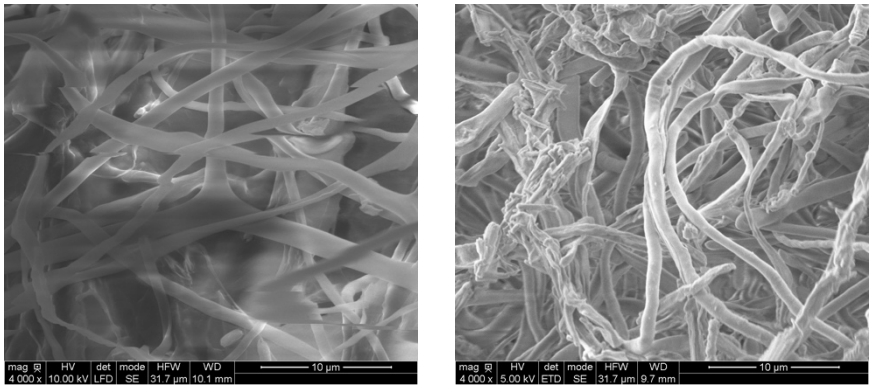

(**a**) (**b**)

Figure 1. High-magnification (G = 4000) observation of mycelium development in the material: (**a**) GHOP; (**b**) VHOP.

At lower magnification, the mycelium network appears denser in *Ganoderma lucidum* (Figure 2). Given that the substrate is the same in both samples, this suggests that hemp shiv granules may not support the development of *Trametes versicolor* as effectively. The denser fungal growth in *Ganoderma*-based sample results in less porosity of that is further discussed in the next section with respect to its effects on hygric and thermal properties.

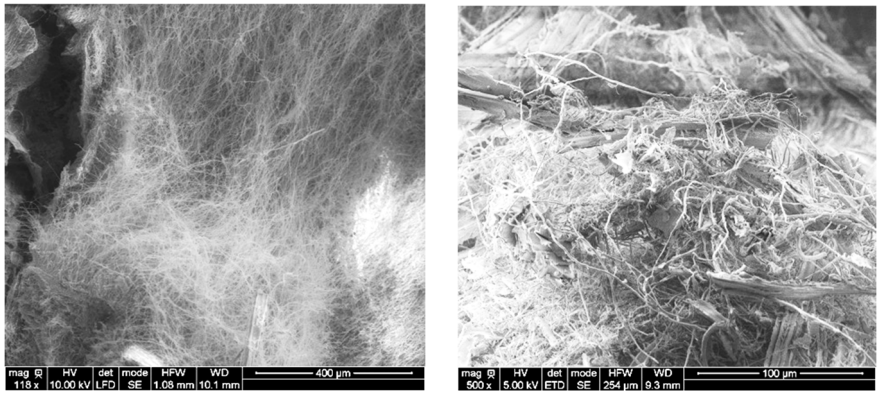

(**a**) (**b**)

Figure 2. Low-magnification (120 < G < 500) observation of mycelium network: (**a**) GHOP (118×); (**b**) VHOP (500×).

While still at a low magnification, the mycelial distribution within the composite appears more extensive and interconnected in the case of *Ganoderma lucidum* (Figure 3c). The denser, tightly interwoven filaments effectively fill voids between hemp granules, creating a more cohesive matrix. This suggests that *Ganoderma lucidum* exhibits stronger substrate colonization, enhancing particle adhesion and overall composite integrity compared to *Trametes versicolor*. However, it is important to note that the samples were observed at different magnifications, which may influence the perceived differences in network density.

While *Ganoderma lucidum* shows a higher concentration of mycelial filaments, both samples exhibit variations in mycelium distribution across different regions. The mycelial growth is notably denser along the edges of the aggregates (Figure 4), suggesting uneven colonization within the composite structure.

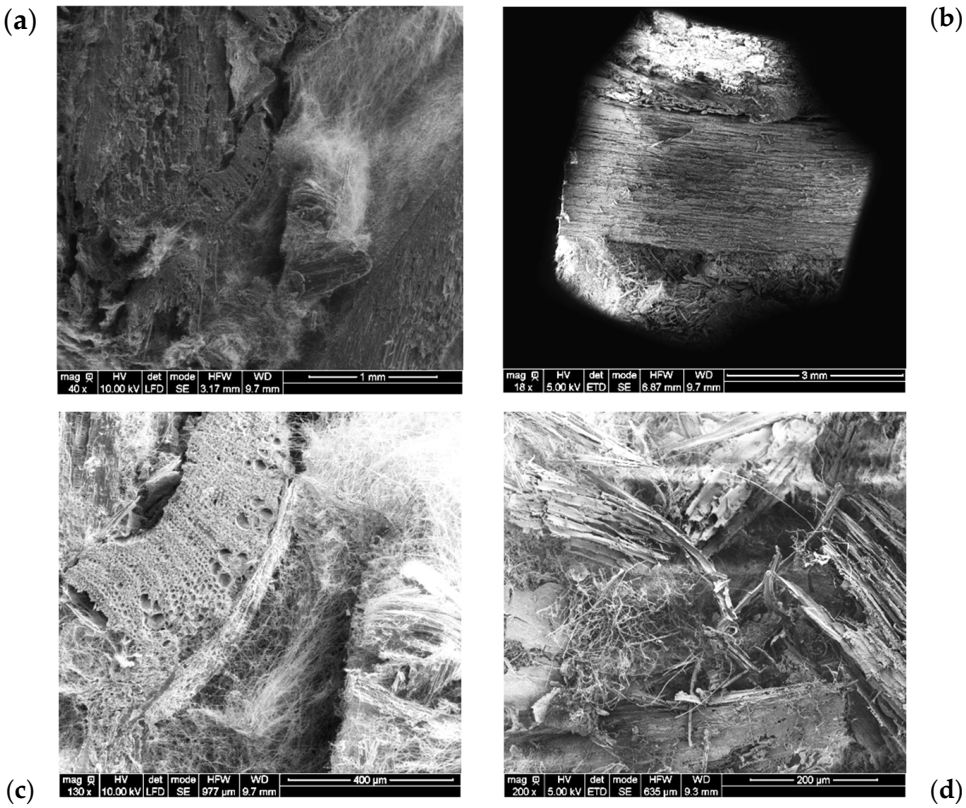

Figure 3. Low-magnification distribution of mycelium throughout the substrate: (**a**) GHOP (30×); (**b**) VHOP (18×); (**c**) GHOP (130×); (**d**) VHOP (200×).

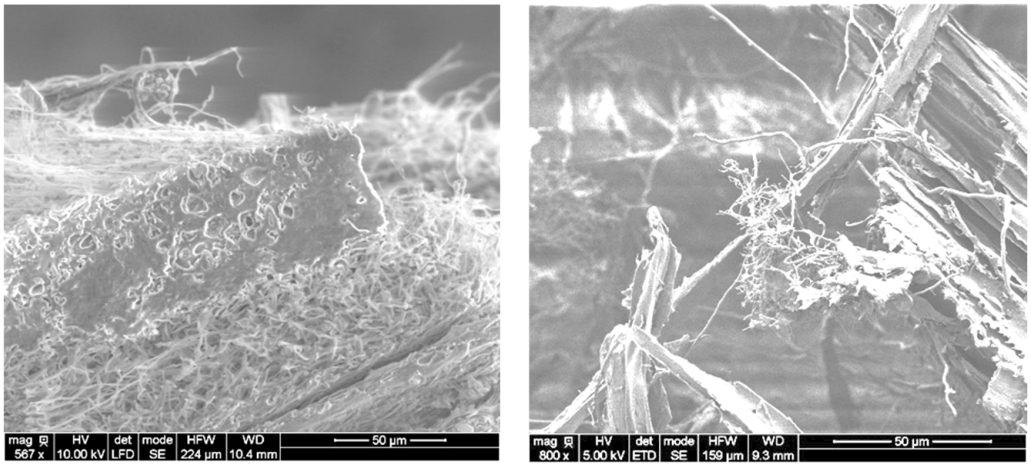

Figure 4. High-magnification distribution of mycelium throughout the substrate: (**a**) GHOP (567×); (**b**) VHOP (800×).

It is also observed that the mycelium does not penetrate the internal structure of the aggregates (Figure 5). This is beneficial, as the retained voids enhance the material's insulating properties by reducing thermal conductivity.

Additionally, at high magnifications, as shown in Figure 6, the presence of mycelium on the surface of the granules suggests partial lignocellulose digestion by the fungus. This interaction indicates the fungus' ability to break down and adhere to the substrate, potentially influencing the material's mechanical properties. The presence of mycelium is notably more pronounced in *Ganoderma lucidum*, suggesting a stronger enzymatic activity or surface colonization compared to *Trametes versicolor*.

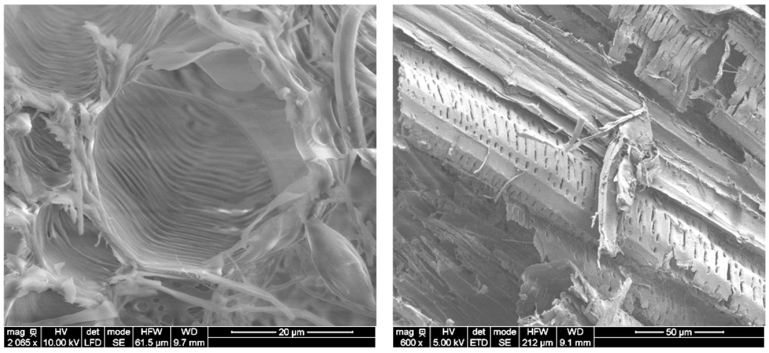

(**a**) (**b**)

Figure 5. Penetration of mycelium into the substrate in high magnification ratio: (**a**) GHOP (2065×); (**b**) VHOP (600×).

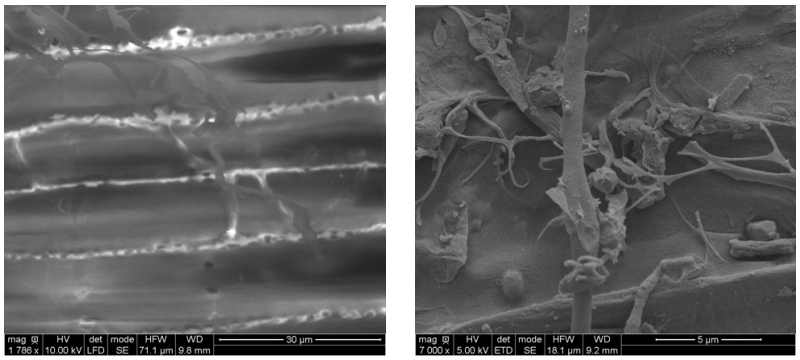

(**a**) (**b**)

Figure 6. Observation of the surface of hemp substrate: (**a**) GHOP (1786×); (**b**) VHOP (7000×).

Additionally, partially spherical or granular structures observed on the granules appear to be part of the mycelium network. According to Adaskaveg and Gilbertson [22], and Gaff M. et al. [23], these formations are likely chlamydospores, specialized fungal structures known for their resistance to harsh conditions such as drought and high temperatures. Their presence suggests a potential adaptation mechanism that enhances the mycelium's ability to survive in challenging environmental conditions. Despite this fungal activity, the substrate's cell walls retain their fundamental morphology, indicating that while the mycelium interacts with the substrate, it does not significantly alter its structural integrity.

While these SEM observations reveal clear differences in network formation and substrate colonization, their functional implications on moisture-related behavior warrant further analysis.

3.2. Hygric Characterization

To evaluate how these structural differences influence the material's response to humidity, we now examine the hygric behavior of MBCs through sorption, permeability, and water uptake tests.

3.2.1. Sorption Isotherms

This test aimed to evaluate moisture sorption behavior, using five formulations (GHOP, GHOU, GHWU, GSWP, and VHOP), using the DVS device. Additionally, adsorption isotherms are tested separately for five temperatures. The sorption isotherms indicate the evolution of moisture content as a function of relative humidity. Figure 7 illustrates Sorption isotherms measured at 23 °C, comparing the effects of mycelium, treatment, substrate, and additive types on sorption across relative humidity levels for the tested formulations.

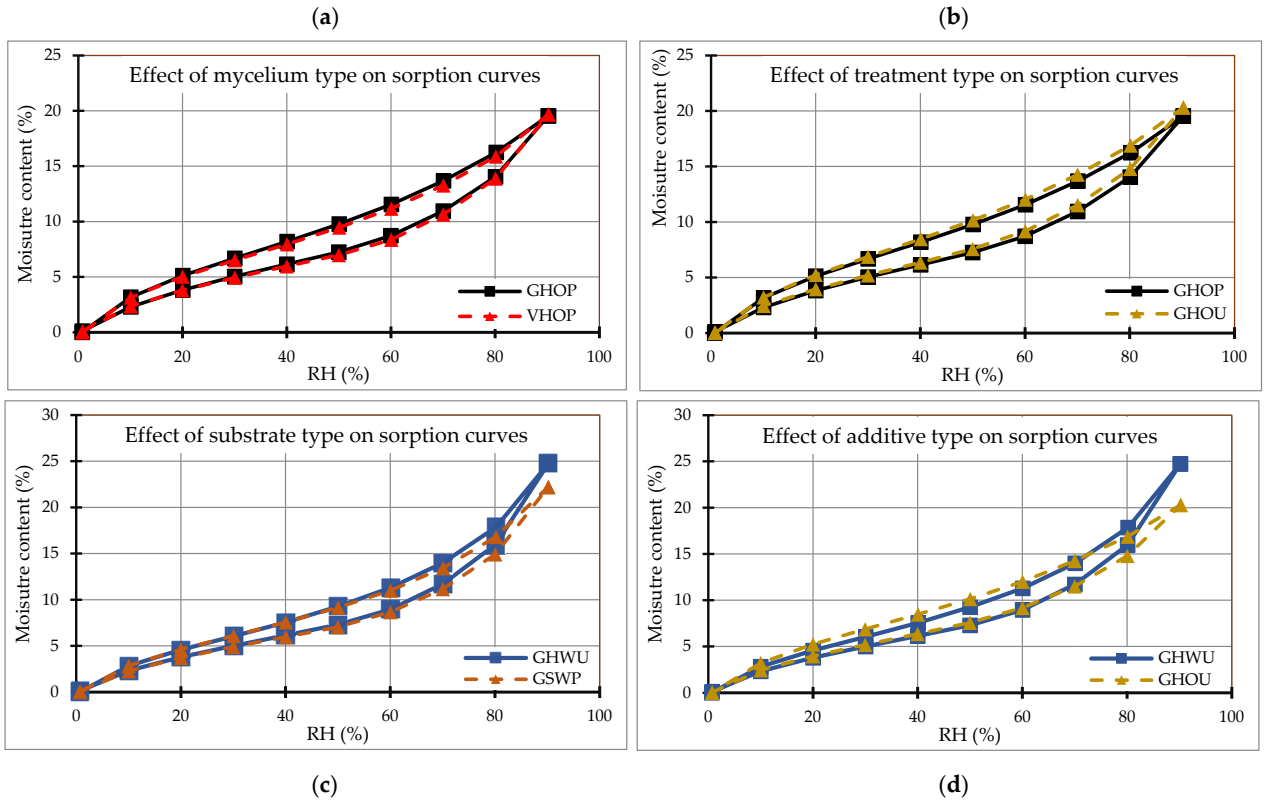

Figure 7. The effect of fabrication parameters on sorption isotherms including: (**a**) mycelium type; (**b**) treatment type; (**c**) substrate type; (**d**) additive types.

The four sorption isotherm graphs reveal that the additive type has the most significant impact on hygroscopic behavior, with GHWU (with additives) showing a 21.82% higher moisture uptake than GHOU (without additives) at 90% RH, followed by substrate type, where GHWU (hemp-based) exhibits an 11.38% higher uptake than GSWP (straw-based) at 90% RH. Treatment type (GHOP vs. GHOU) has a smaller effect, with a maximum difference of 5.28% at 80% RH, while mycelium type (GHOP vs. VHOP) shows the least impact, with GHOP's uptake only 4.34% higher than VHOP's at 60% RH. An initial interpretation of the negligible sorption difference observed between GHOP and VHOP can be drawn from SEM images, which show strong surface colonization by both species. The presence of chitin in the mycelial structures may increase surface hydrophobicity, potentially resulting in similar moisture interactions under the low-pressure, laminar airflow conditions of the DVS device. However, a more detailed analysis of the internal microstructure provides deeper insight into this behavior.

These findings can be further understood by referring to the microstructural observations presented in Section 3.1. Although the difference in moisture uptake between GHOP and VHOP is quantitatively small (4.34% at 60% RH), the structural analysis provides valuable insights into this behavior. SEM images (Figures 2–4) revealed that *Ganoderma lucidum* forms a denser and more interconnected hyphal network compared to *Trametes versicolor*, which tends to produce a looser and more localized structure. The denser network in GHOP likely enhances connectivity between internal pores while simultaneously limiting their volume, thus reducing capillary condensation at high RH. Conversely, the more porous VHOP structure may offer more adsorption sites but with reduced interconnectivity, leading to localized saturation that does not lead to an increased total moisture content under DVS conditions.

Furthermore, the relatively higher sorption observed in hemp-based composites (e.g., GHWU) compared to straw-based ones (e.g., GSWP) is consistent with differences in fungal

colonization efficiency. SEM images showed more homogeneous mycelial development in hemp composites, whereas straw-based composites exhibited anisotropic colonization and incomplete coverage of intergranular spaces. This results in less effective moisture transport pathways and a reduced capacity for homogeneous moisture distribution throughout the material volume, despite higher open porosity values.

The pronounced effect of additives, as observed in GHWU, also aligns with microstructural trends. Nutritional supplements enhance fungal activity and hyphal proliferation, increasing the overall surface area available for moisture interaction. This may also contribute to more complex capillary networks within the composite, leading to increased moisture retention at higher RH levels. These relationships between structure and moisture response are summarized in Figure 8 below, where the correlation between microstructure and hygroscopic behavior in mycelium-based composites is highlighted. The SEM micrographs show the dense, interconnected hyphal network of *Ganoderma lucidum* (top) and the more porous, localized structure of *Trametes versicolor* (bottom). The corresponding sorption isotherms illustrate slightly higher moisture uptake in GHOP due to network interconnectedness, and significantly increased uptake with additive use (GHWU), indicating a higher hygroscopic capacity associated with enhanced surface area.

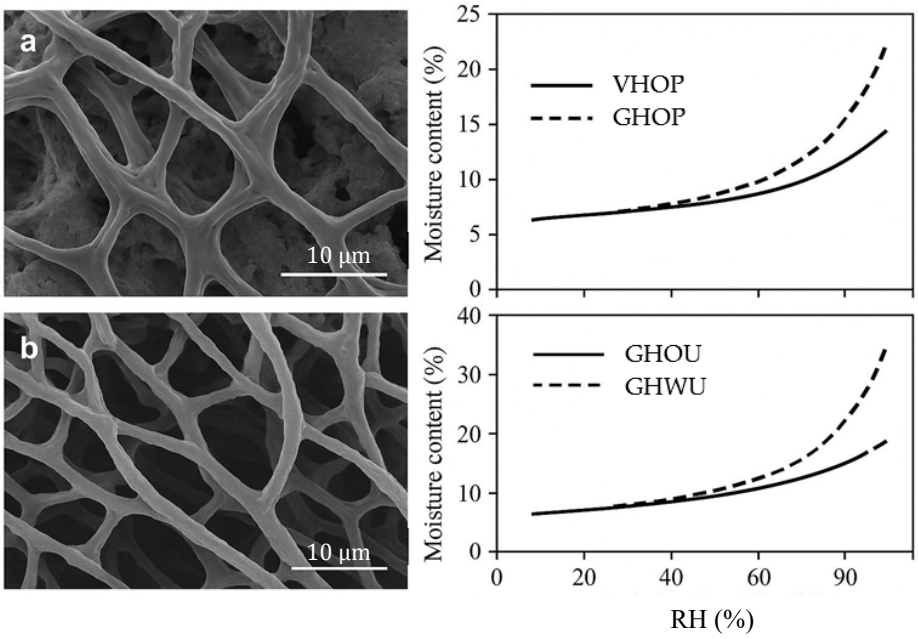

Figure 8. Correlation between microstructure of (**a**) *Ganoderma lucidum* and (**b**) *Trametes versicolor* and hygroscopic behavior in mycelium-based composite.

In light of these correlations, it becomes evident that sorption behavior in mycelium-based composites is governed not only by the total porosity or fungal species but by the spatial configuration and connectivity of the hyphal network formed during colonization. Integrating microstructural features into the interpretation of hygric measurements offers a more comprehensive understanding of moisture dynamics and supports the hypothesis that controlling fungal morphology through fabrication parameters is key to tailoring MBC performance for building applications.

GAB model was applied to fit the experimental adsorption isotherms of formulations enabling a quantitative assessment of their hygroscopic behavior across the full range of relative humidity at 23 °C. According to Equation (1), the calculated values of the GAB parameters are presented in Table 2 as follows.

Table 2. Fitting constants of the sorption isotherms based on GAB equation at 23 °C.

Sample	Type	Fitted GAB Parameters		
		w (kg/kg)	c	k
GHWU	Adsorption	0.053	8.701	0.877
GSWP	Adsorption	0.054	8.727	0.848
GHOP	Adsorption	0.062	8.412	0.772
VHOP	Adsorption	0.057	9.596	0.798
GHOU	Adsorption	0.066	7.825	0.768

The GAB model parameters also reveal significant distinctions: GHOP and GHOU exhibit higher monolayer moisture content values than VHOP, indicating a stronger initial affinity for moisture. This supports the hypothesis that the presence of chitin in *Ganoderma lucidum* (as confirmed by Yang et al. [12]) increases surface hydrophobicity, while also creating internal zones that favor multilayer adsorption under high relative humidity conditions.

Figure 9 compares the GAB equation fittings with experimental adsorption isotherms, evaluating the effects of mycelium, substrate, treatment, and additive types on moisture content as a function of relative humidity.

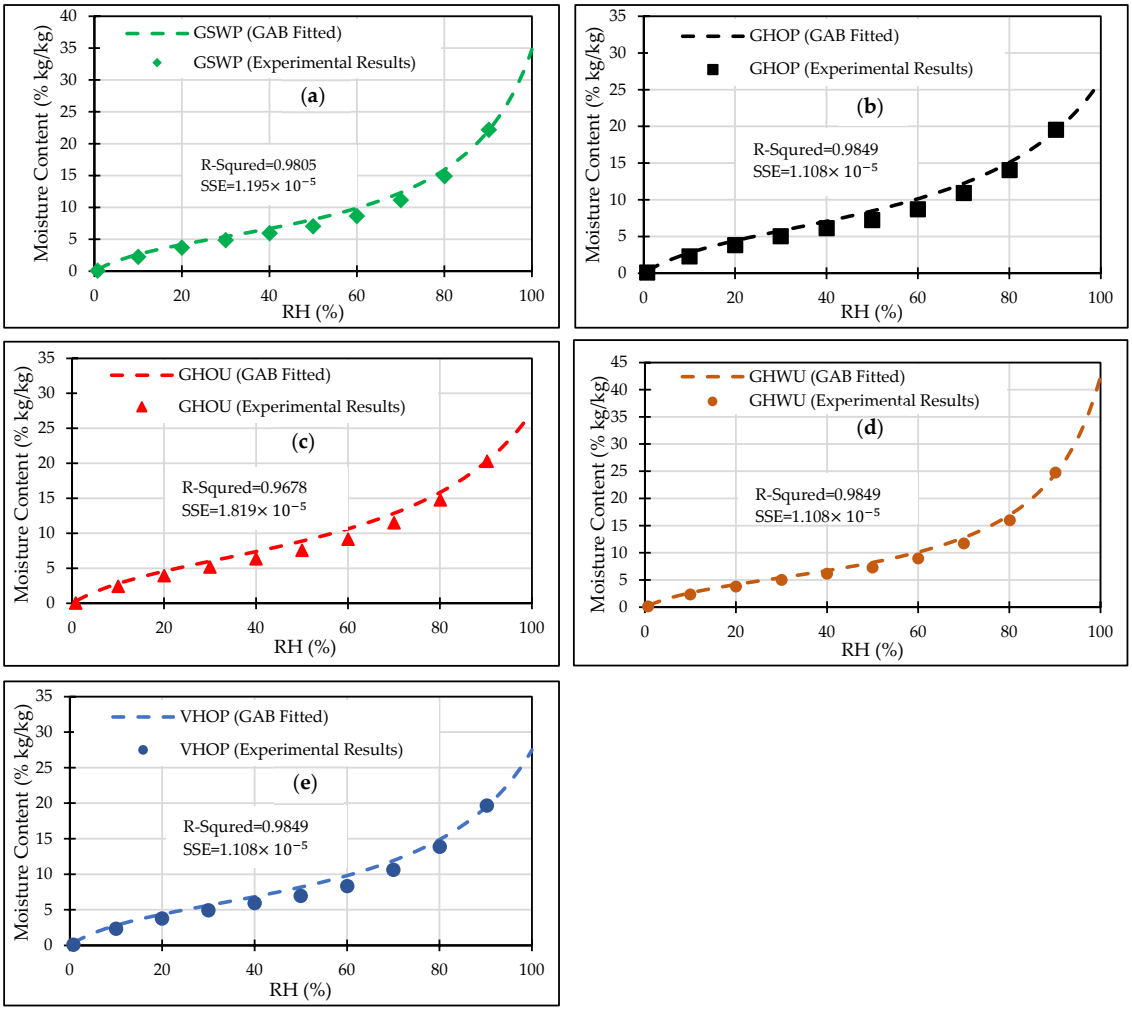

Figure 9. Comparison of GAB equations fitting with experimental adsorption isotherms: (**a**) GSWP; (**b**) GHOP; (**c**) GHOU; (**d**) GHWU; (**e**) VHOP.

The GAB equation effectively captures the hygroscopic behavior of the tested MBC formulations, as demonstrated by high R-squared values (0.9678–0.9849) and low sum of squared errors (SSE ranging from 1.108×10^{-5} to 1.956×10^{-5}), indicating a strong fit between the model and experimental data across all relative humidity levels.

Figure 10 compares the adsorption isotherms for the GHWU formulation at five temperatures (15 °C, 23 °C, 30 °C, 35 °C, and 40 °C) to assess the impact of temperature on moisture storage capacity across relative humidity levels. The DVS device restricts high RH measurements at elevated temperatures because generating and controlling high humidity becomes technically unstable and physically constrained due to the exponential increase in vapor pressure, risk of condensation, and sensor limitations. This is a common constraint across most gravimetric sorption analyzers.

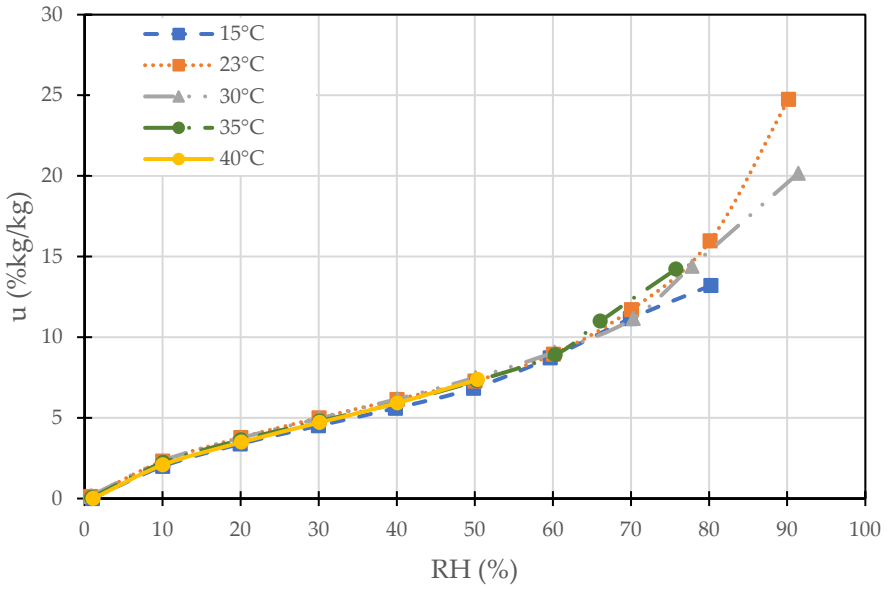

Figure 10. Experimental adsorption isotherms' comparison in different temperature for GHWU.

The isotherms show moisture content stable at 0–5% up to 60% RH, rising to 25–30% at 90% RH across all temperatures, indicating that temperature has minimal impact on storage capacity (kg/kg). Generally, at higher temperatures (35 °C and 40 °C), there is a slight increase in adsorbed moisture, possibly due to the small widening of pores. However, since this material is already highly porous, temperature does not significantly alter its internal structure, resulting in only minor changes in moisture adsorption. This finding differs from the hygric behavior of other insulation materials, where temperature typically affects moisture sorption more significantly, suggesting the need for further validation tests with additional formulations to confirm this behavior. The substantial rise in sorption isotherms at higher relative humidity levels is primarily attributed to the increased availability of moisture content, in the air at higher temperatures.

3.2.2. Permeability

This test aimed to assess vapor permeability under 0/50% and 0/80% RH gradients using three formulations (GSWP, GHWU, and VSOP). For each mixture, three samples were tested, and the results are illustrated in Figure 11. A linear curve fitting is performed to indicate the evolution of moisture within the materials. Although the steady state was reached at the 150 h mark of the test, the test continued until the 315th hour. Consequently, a linear curve fit was applied to the data from this point onward, excluding the initial steep increase in moisture observed during the first 20 h.

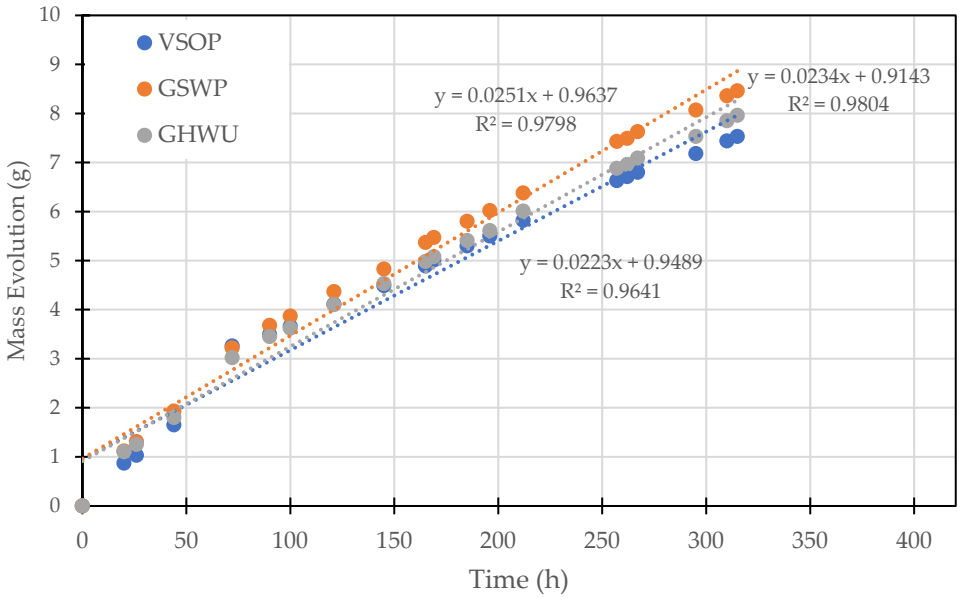

Figure 11. Adsorbed moisture evolution in the dry cup condition (0/50%).

Using Equations (2) and (3), the vapor permeability and resistance factors are calculated from known vapor pressure and mass flow rate values, as shown in Table 3. This result confirms the higher permeability in the composition of straw and *Ganoderma lucidum* (GSWP) compared to straw and *Trametes versicolor* (VSOP) as well as hemp and *Ganoderma lucidum* (GHWU) samples, although their values remain very close. For the 0/80 relative humidity gradient case, the resistance factor decreased by approximately 22% for VSOP, 28% for GSWP, and 30% for GHWU.

Table 3. Water vapor permeability and resistance factors.

Composite	RH [%]	$g_v \times 10^6$ [kg·m^{-2}·s^{-1}]	$\delta_p \times 10^{11}$ [kg·m^{-1}·s^{-1}·Pa^{-1}]	μ
GHWU	0/50	1.097	1.57	12.73
	0/80	1.57	2.25	8.91
GSWP	0/50	1.223	1.74	11.50
	0/80	1.70	2.42	8.29
VSOP	0/50	1.022	1.45	13.77
	0/80	1.34	1.87	10.68

These results can be further interpreted in light of the aforementioned microstructural observations. While vapor permeability is commonly associated with overall porosity, the pore connectivity and hyphal architecture could play an equally critical role in driving moisture vapor transport through mycelium-based composites.

SEM imaging revealed that *Ganoderma lucidum* develops a dense, continuous hyphal network that forms highly connected pathways between substrate particles. In the case of straw-based composites like GSWP, this structure not only preserves pore interconnectivity but also stabilizes the pore geometry, preventing collapse during drying and thereby supporting efficient vapor diffusion. This explains the relatively high permeability observed in GSWP, despite the potentially lower overall porosity compared to VSOP.

Conversely, *Trametes versicolor* exhibits a more fragmented and localized colonization pattern, as shown in Figure 3, which leads to discrete pore zones that are poorly interconnected. Although this may result in a higher total porosity (as inferred from VHOS free

water saturation results), the lack of continuity between voids severely limits vapor transfer, increasing the vapor diffusion resistance factor μ. This supports the idea that "effective porosity"—i.e., the fraction of pore space that contributes to bulk transport, is more relevant than absolute porosity when interpreting vapor permeability in bio-based composites.

Moreover, the combination of straw substrate and nutritional additives in GSWP likely enhanced both fungal growth intensity and structural uniformity, further contributing to an optimal balance between pore size, distribution, and connectivity. This may explain why GSWP shows not only higher vapor permeability than VSOP but also a sharper decrease in μ under 0/80% RH conditions, reflecting improved moisture transport even under elevated humidity gradients.

3.2.3. Liquid Conduction Coefficient

This test aimed to determine the capillary adsorption behavior of mycelium bio-composites and calculate the subsequent liquid conduction coefficients, using three formulations (GSWP, GHOU, GHOP) with three samples per formulation. Figure 12 shows the capillary adsorption of these composites by plotting the average mass difference against the square root of time.

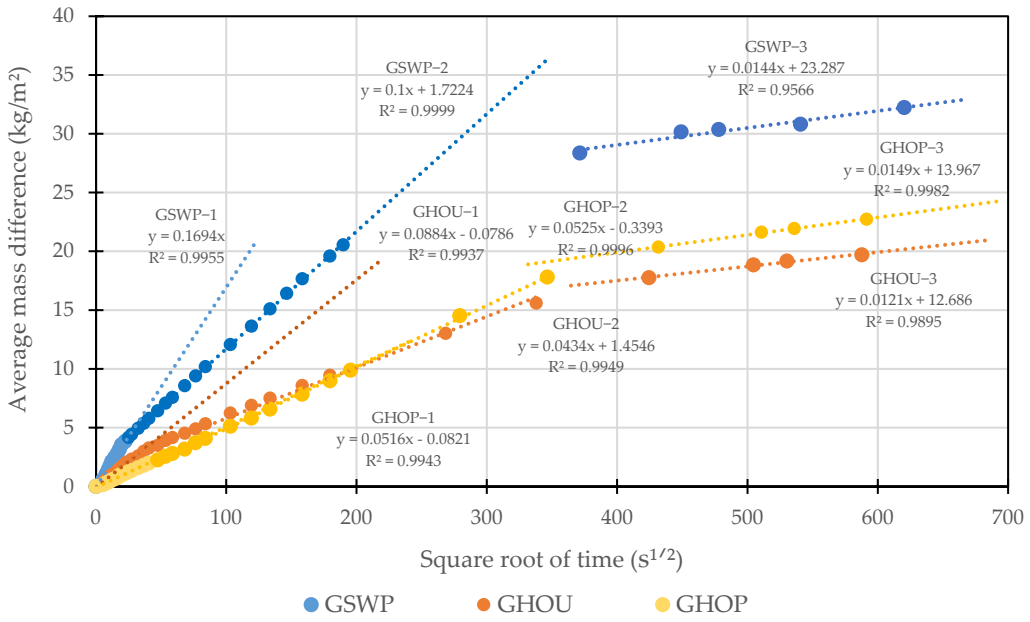

Figure 12. Capillary adsorption of mycelium bio-composites.

As capillary absorption phenomena are diffusive in nature, Figure 12 demonstrates that the initial evolution follows a linear trend relative to the square root of time. The coefficients of capillary adsorption (A_c) correspond to the slopes of the fitted trend lines. These coefficients are quite different for the straw and *Ganoderma* (GSWP) composite (A_c = 0.16 kg·m^{-2}·s$^{-1/2}$), as the largest value is three times the hemp and *Ganoderma* (GHOP) composite (A_c = 0.0516 kg·m^{-2}·s$^{-1/2}$).

These results corroborate the findings of Rahim et al. [24], who reported that the capillary coefficient of straw lime concrete (SLC) is four times higher than that of hemp lime concrete (HLC). While the capillary coefficients of SLC and straw-based Ganoderma composites (GSOP) are comparable, hemp-based Ganoderma composites (GHOP) exhibit higher values than HLC. This increase may be attributed to the robust growth of Ganoderma in hemp-based composites compared to lime-based composites, leading to the formation of larger pores within the material, which in turn elevates the capillary coefficient.

3.2.4. Free Water Saturation

Free water saturation testing was conducted to quantify the open porosity and water retention capacity of the mycelium-based composites. By submerging samples in water under controlled conditions, this test evaluates how effectively each formulation absorbs and retains water, thereby providing critical insights into pore structure and hygrothermal performance. Eight formulations were analyzed to assess the effects of key parameters, including fungal species, substrate type, and treatment, on water uptake. Table 4 presents the water content results of the studied materials.

Table 4. Physical characteristics of mycelium-based composites.

Samples	Density (kg/m^3)	Free Water Saturation (kg/m^3)	Free Water Saturation (%)	Open Porosity (%)
GHOP	152 ± 3	886 ± 27	580 ± 10	85 ± 0
GHOS	131 ± 0	920 ± 14	701 ± 12	88 ± 0
GHWU	212 ± 4	809 ± 17	382 ± 15	79 ± 1
GSOS	170 ± 4	945 ± 35	556 ± 33	85 ± 1
GSWP	223 ± 15	833 ± 15	375 ± 28	79 ± 1
GSWS	188 ± 3	893 ± 12	475 ± 12	83 ± 0
VHOS	142 ± 13	1000 ± 63	704 ± 19	88 ± 0
VSOP	184 ± 13	818 ± 20	447 ± 41	82 ± 1

The values reported in Table 4 reinforce and contextualize the observed hygrothermal trends by providing insight into the relationship between fungal morphology, substrate structure, and the water storage behavior of MBCs. Formulations such as GHOP (*Ganoderma lucidum* on hemp) display a relatively high dry density (152 kg/m^3) combined with lower open porosity (85%) and moderate free water saturation (580%), reflecting the densely interwoven hyphal network observed under SEM (Figures 2 and 3). This compact structure minimizes void volume and inhibits water penetration, contributing to low capillary adsorption coefficients (Figure 12) and moderate sorption capacity at high RH (Figure 7a).

In contrast, VHOS demonstrates higher open porosity (88%) and water saturation (704 kg/m^3), which aligns with the fragmented and loosely connected hyphal growth observed in and Figure 4. This architecture results in numerous isolated or dead-end pores that facilitate high water uptake but offer limited resistance to moisture transport. Despite this high porosity, the sorption isotherms for VHOP (Figure 7a) show only moderate moisture content under DVS conditions, indicating that vapor-phase sorption is hindered by the lack of continuous pathways and the localized nature of hyphal development.

Additive-enriched formulations (e.g., GHWU and GSWP) tend to exhibit denser internal organization and reduced capillary sorption behavior (Figure 12), likely due to enhanced fungal colonization and greater hyphal branching. These formulations show lower free water saturation levels (375–382 kg/m^3) and display more gradual sorption curves, as seen in GHWU (Figure 7d). This suggests that while additives increase the surface area for vapor adsorption, they concurrently limit rapid liquid infiltration, likely by reducing large, continuous pore channels.

Straw-based composites such as GSWS and GSOS exhibit both higher porosity (up to 88%) and elevated free water saturation, indicating a greater susceptibility to capillary water uptake and bulk saturation. This behavior stems from the less compact and more heterogeneous structure of straw particles, which promote uneven fungal growth and larger void spaces. As shown previously, the capillary uptake coefficient for GSWP is more

than three times higher than that of GHOP, confirming the dominant influence of substrate morphology on liquid-phase water transport.

Overall, these findings demonstrate that water retention in MBCs is governed not only by open porosity, but by the geometry, connectivity, and functionality of the internal pore network, all of which are shaped by fungal species, substrate type, and processing parameters. A dense, well-integrated hyphal structure minimizes moisture sensitivity and favors stable performance, while porous, loosely organized networks permit high water uptake but compromise material durability. This highlights the necessity of tailoring microstructural features to achieve optimal hygrothermal responses for insulation applications.

Figure 13 illustrates the correlation between open porosity and density, revealing a reverse linear relationship in most samples, except for VHOS which exhibits a different pattern. This suggests that a significant portion of the porosity in these materials is open. This is largely due to the fabrication process of mycelium-based samples, where the growth of fungi within the substrate releases gases that can create open pores during formation. Based on this finding, substituting w_{max} with w_f minimally affects the results.

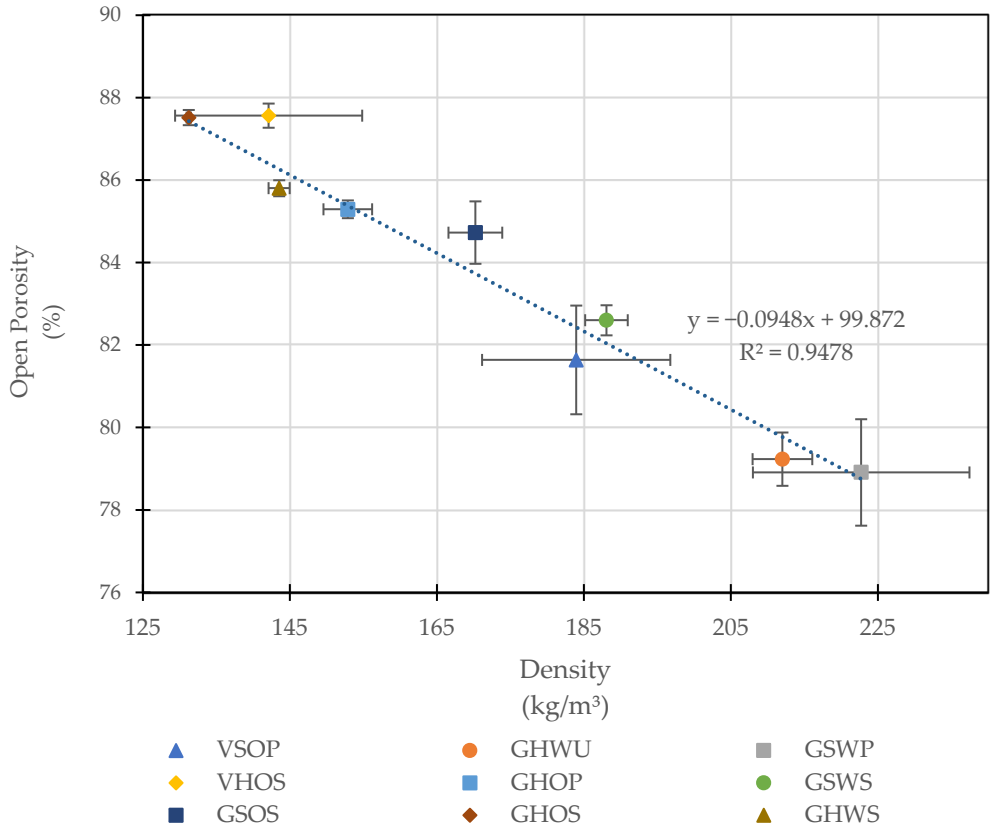

Figure 13. Open porosity and density correlation.

Figure 13 illustrates a general inverse relationship between open porosity and dry density, confirming that denser composites tend to have fewer accessible voids. This trend reflects the effect of fungal colonization: dense hyphal networks, particularly in *Ganoderma lucidum*-based formulations like GHOP and GHWU, enhance particle cohesion and reduce pore volume. However, deviations from this trend, such as in VHOS, suggest that species-specific growth patterns; here, the fragmented colonization by *Trametes versicolor* can produce highly porous but structurally loose composites. These discrepancies highlight that porosity is influenced not only by compaction, but also by pore connectivity and distribution.

The observed structural configurations, shaped by fungal species and substrate interactions, are crucial for interpreting the material's thermal behavior. As moisture retention and transport directly affect heat flow, understanding these microstructural differences provides a foundation for evaluating the thermal performance of MBCs under realistic environmental conditions.

3.3. Thermal Characterization

The interplay between density, open porosity, and moisture retention confirms that thermal behavior in MBCs cannot be dissociated from their hygric and microstructural characteristics. The replacement of air by adsorbed or capillary-bound water within the pore network, governed by hyphal morphology, substrate structure, and pore connectivity, directly impacts thermal conductivity. Thermal transport must be interpreted as the outcome of coupled heat and mass transfer processes, modulated by the material's internal architecture.

Thus, thermal characterization was performed to assess the heat transfer properties of the mycelium-based composites as a function of relative humidity, moisture content and temperature to evaluate the individual and combined effects of each parameter on thermal performance. Utilizing the TPS method, key formulations, including GHOP, GSWS, GSOS, and VHOS, were evaluated to establish a quantitative correlation between microstructural features and thermal conductivity.

The correlation between thermal conductivity and temperature across different levels of relative humidity is demonstrated in Figure 14 for four samples. This expansion may enhance gaseous conduction within the pores, thereby directly contributing to an increase in thermal conductivity. However, it should be noted that the overall thermal response is also influenced by changes in moisture content and other material properties. As delineated in Equation (8), temperature increase corresponds to an exponential elevation in saturation pressure. Consequently, under constant relative humidity (RH) within the climatic chamber, as a result of temperature increase, vapor pressure experiences a proportional rise. This explains the indirect consequence of temperature elevation, in increasing the moisture content stored within the material.

In all four composites (VHOS, GHOP, GSOS, and GSWS), thermal conductivity increases with both temperature and relative humidity, confirming the dominant role of moisture in enhancing heat transfer by replacing air within the pore network. However, the magnitude and progression of this increase vary significantly depending on the material's microstructure.

GHOP displays the most stable thermal response, with only a modest rise in conductivity. This behavior reflects the dense and cohesive hyphal network observed, which not only limits overall moisture uptake, as confirmed by low capillary absorption and moderate sorption levels, but it also prevents pore dilation under thermal stress. As a result, the pore geometry and gas-filled structure remain largely preserved, maintaining low thermal conductivity even under elevated RH and temperature.

In contrast, VHOS exhibits a steeper and more nonlinear increase in thermal conductivity. This correlates with its high free water saturation and fragmented, porous hyphal morphology (Figure 4b), which allows for extensive moisture accumulation and dynamic pore reconfiguration. The loosely organized microstructure lacks the structural rigidity to resist thermal expansion of moisture-laden pores, amplifying the composite's sensitivity to environmental changes.

Straw-based samples such as GSOS and GSWS occupy intermediate positions. Despite also being colonized by *Ganoderma lucidum*, their higher thermal conductivity variation can be attributed to the more heterogeneous and anisotropic colonization of the straw substrate, which creates larger, less confined pores with enhanced moisture transport capacity. This

substrate-driven irregularity disrupts the structural integrity of the hyphal matrix, resulting in localized zones of high moisture accumulation and increased conductive pathways as temperature rises.

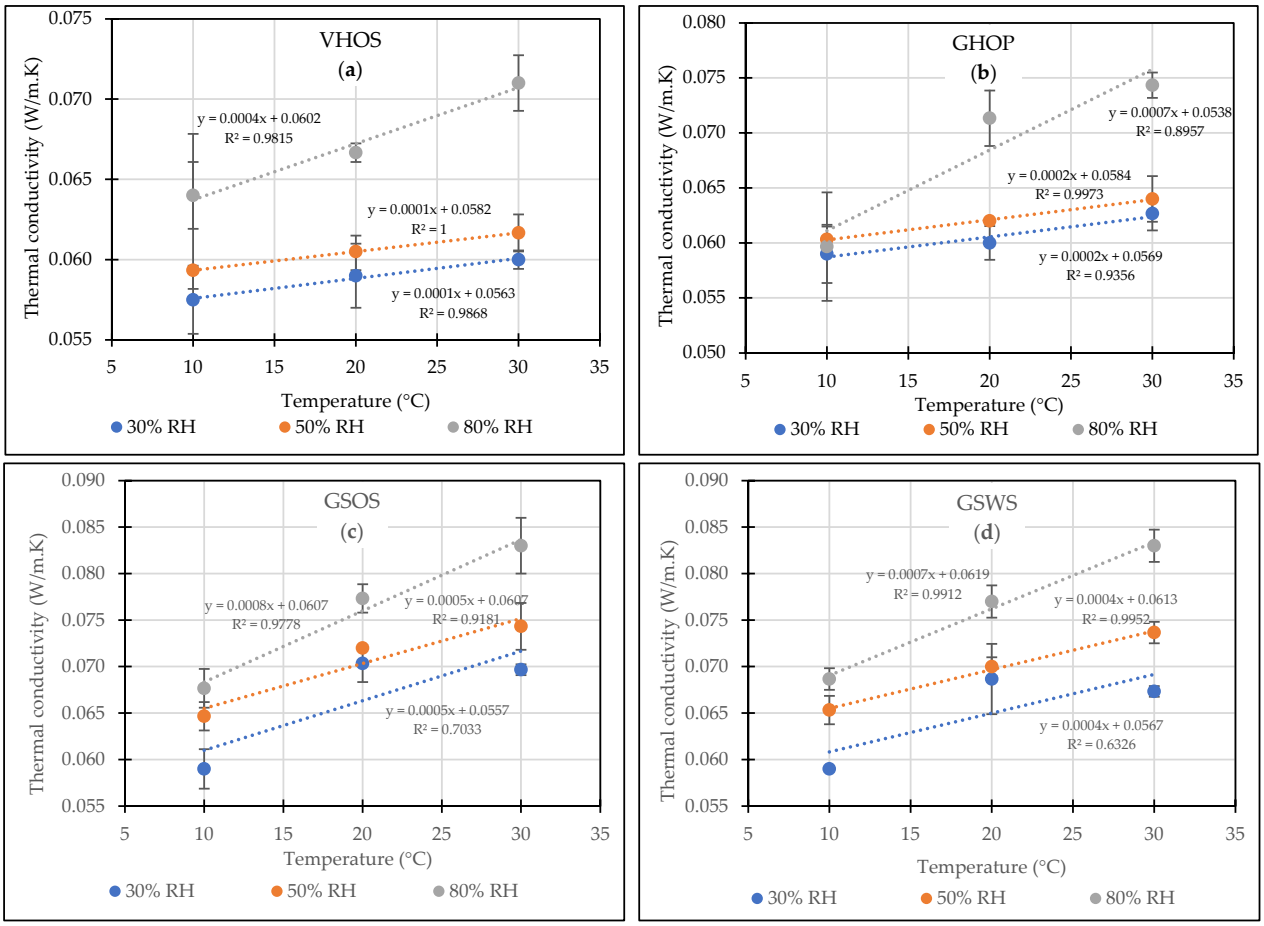

Figure 14. Correlation between thermal conductivity and temperature across different relative humidities for: (**a**) VHOS; (**b**) GHOP; (**c**) GSOS; (**d**) GSWS.

Altering relative humidity causes fluctuations in moisture content, thereby directly impacting thermal conductivity. The influence of relative humidity on thermal conductivity at various temperatures is illustrated in Figure 15. At lower temperatures, there is minimal change in thermal conductivity across different RH levels, due to the low saturation pressure and subsequent low vapor pressure in all RH levels. At 30% RH, the lowest achievable level within the climatic chamber, thermal conductivity values tend to converge. However, as RH increases up to 80%, differences between thermal conductivity at various temperatures become more pronounced due to increased disparities in moisture content. Additionally, increasing temperature amplifies the increase in thermal conductivities at constant RH levels by increasing moisture content through higher saturation vapor pressure.

In order to better understand the behavior of thermal conductivity as the function of temperature and moisture content, a curve fitting is conducted using MATLAB R2024b. Due to the steeper change in thermal conductivity against moisture content, compared to temperature in the conducted experiments, moisture content is treated as the exponential variable in the correlation, while temperature is considered part of the linear component. The three possible exponential models that could be implemented are as follows:

- $k = a + b \cdot T + c \cdot e^{d \cdot u}$ (Model 1),

- $k = (a + b \cdot T) \cdot e^{c \cdot u}$ (Model 2),
- $k = a + b \cdot T \cdot e^{c \cdot u}$ (Model 3),

Where k denotes thermal conductivity, T represents temperature, and u is the moisture content. Model 1 captures the cumulative effects of moisture and temperature. It performs well but slightly underestimates thermal conductivity at higher temperature and moisture content. Models 2 and 3's multiplicative forms better reflect the combined influence of moisture content and temperature. However, Model 2 yields a higher R-Squared and lower RSS, suggesting a better fit for this dataset. Therefore, Model 2 is chosen for the curve fitting. The resulting curve fitting is depicted in Table 5.

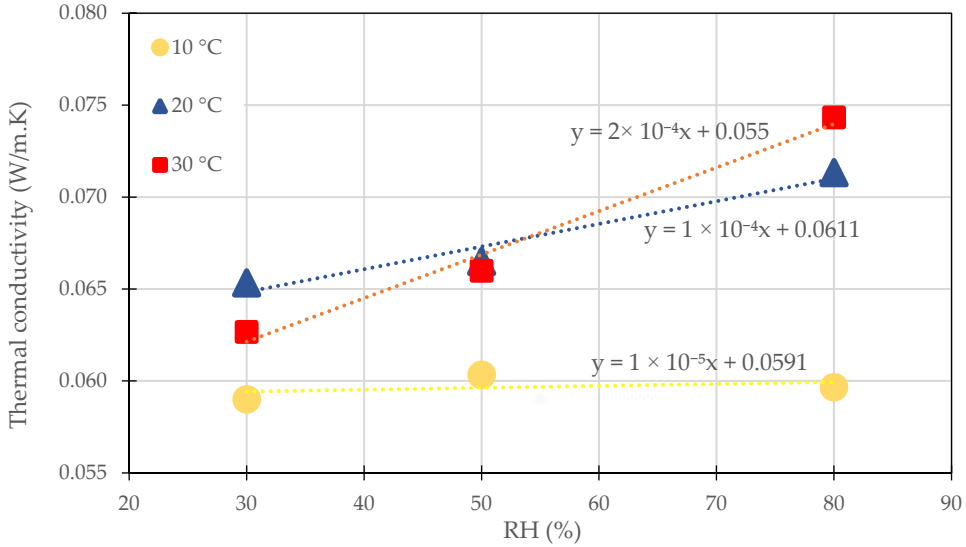

Figure 15. Correlation between thermal conductivity and relative humidity in constant temperature for GHOP.

Table 5. Thermal conductivity correlation as a function of the moisture content (kg/kg) and temperature (K).

Composite	Curve Fitting	R-Squared	RMSE
GHOP	$y = (0.0008 + 0.0005\mathrm{T}) \times (0.3812 \times \exp(1.2771u))$	0.6883	0.0037
GSWS	$y = (0.0042 + 0.0137\mathrm{T}) \times (0.0155 \times \exp(1.9552u))$	0.8803	0.0031
GSOS	$y = (0.004 + 0.0154\mathrm{T}) \times (0.0139 \times \exp(1.8016u))$	0.8421	0.0035
VHOS	$y = (0.02 + 0.0164\mathrm{T}) \times (0.0118 \times \exp(1.3971u))$	0.8136	0.0023

The exponential fitting parameters presented in Table 5 quantify how each composite's thermal conductivity (k) responds to temperature (T) and moisture content (u), which can be directly related to their microstructural organization and moisture dynamics. In porous biocomposites, k is the sum of solid-phase conduction through the hyphal skeleton (k_s), gas-phase conduction in air-filled pores ($k_g \approx 0.026$ W m^{-1} K^{-1}), bound-/liquid-water conduction ($k_w \approx 0.6$ W m^{-1} K^{-1}), and a minor radiative term. Rising temperature dilates the average pore diameter and simultaneously raises saturation vapor pressure; these changes increase k_g and k_w, respectively, thus explaining the upward k(T) trends predicted by the exponential model.

GHOP exhibits the lowest sensitivity coefficients for both temperature (0.0005) and moisture content (1.2771), confirming its thermally stable behavior under varying environmental conditions. This reduced sensitivity aligns with the previously observed dense and cohesive hyphal network, which minimizes internal pore volume variation and limits water

uptake. Such a compact limits both free-air volume and water uptake. Solid-phase conduction therefore dominates, and thermal conductivity varies little with either temperature (T) or moisture content (u).

Conversely, VHOP shows significantly higher sensitivity to both parameters, with a moisture coefficient of 1.3971 and a temperature coefficient of 0.0164. These values reflect the more open and disconnected microstructure formed by *Trametes versicolor*. Its high open porosity (~88% for VHOS; Figure 13) produces macropores that (i) dilate upon heating—enhancing gas-phase conduction—and (ii) rapidly fill with water once capillary condensation begins. The exponential fit to k versus u shows a clear inflection in slope at u $\approx$ 0.15 kg·kg^{-1}, marking the transition from multilayer adsorption to capillary water bridges that is consistent with the sorption isotherm of VHOP (Figure 7a). Beyond this moisture content, liquid-phase conduction ($k_w \approx 0.6$ W·m^{-1}·K^{-1}) dominates, accounting for VHOP's steep k(T, u) response. This supports the findings of the elevated free water saturation observed in VHOS and its pronounced capillary absorption behavior. Straw-based samples (GSOS, GSWS) colonized by *Ganoderma lucidum* exhibit intermediate sensitivity coefficients and a moderate k(T, u) response, positioning them between the two extremes. Although they share the same fungal species as GHOP, their higher sensitivity coefficients (1.8016–1.9552 for moisture) reflect the influence of the straw substrate's inherent heterogeneity. The longitudinal lumina of the straw fragments introduce anisotropic pore channels that promote moisture transport along the fiber axis. It also contributes to localized pore development and variable moisture distribution, leading to less predictable thermal responses. At elevated moisture contents, these channels facilitate the formation of continuous liquid films, enhancing heat conduction through liquid-phase bridging.

Despite the adequacy of the exponential model in capturing general trends, lower R^2 values, particularly for GHOP, may result from experimental limitations such as uneven sample surfaces affecting probe contact, or reduced measurement stability at low moisture contents. Future work could involve re-testing with a guarded hot plate apparatus under steady-state conditions ($\Delta T \leq 10$ K) and will verify the fitted coefficients and overcome limitations associated with surface compressibility in TPS measurements. This will also enable the integration of a three-phase (solid–gas–liquid) conduction model that explicitly couples pore-size distribution with the moisture-sorption isotherms. A similar three-phase framework has been shown to predict increases in thermal conductivity in highly porous aerogels when adsorbed water replaces air in mesopores—facilitating capillary condensation and the formation of liquid bridges that enhance heat transfer [25], thereby supporting the mechanism proposed here.

4. Conclusions and Perspective

4.1. Conclusions

This study examined the hygrothermal behavior of eleven mycelium-based composites (MBCs) fabricated using various fungal strains, fiber types, sterilization levels, and nutrient additives. Among the tested fungal species, Ganoderma lucidum, particularly in the GHOP formulation, demonstrated the lowest k-value (0.045 W m^{-1} K^{-1}), with minimal moisture content and temperature-induced variation, confirming its robustness for bio-based insulation.

Microstructural analysis revealed that *Ganoderma lucidum* forms a compact, interconnected hyphal network, while *Trametes versicolor* produces a more open, porous structure. Extensive hygric and thermal characterizations showed that additives and substrate type had the strongest influence on moisture uptake, whereas fungal species and treatment effects were more modest. GHOP consistently exhibited lower vapor permeability, reduced capillary absorption, and greater thermal stability due to its dense microstructure.

The study highlights a clear relationship between porosity, moisture dynamics, and thermal behavior: denser hyphal networks reduce pore connectivity and moisture ingress, thereby stabilizing thermal conductivity. Elevated open porosity alone did not inherently result in thermal performance; effective insulation was observed when pores were enclosed within a cohesive hyphal matrix, which restricted capillary water uptake and limited temperature-driven increases in thermal conductivity. The exponential model further confirmed that composites with more porous and disconnected structures were more sensitive to vapor pressure increases. This enabled the GHOP formulation to maintain lowest conductivity values across a wide hygrothermal range (10–30 °C and 0–80% RH).

In summary, the study established that the hygrothermal performance of MBCs is governed by the geometry and connectivity of their internal structure, shaped by fungal selection and processing parameters. By optimizing these features, MBCs can be tailored for reliable, energy-efficient insulation, supporting their practical adoption in sustainable construction.

4.2. Perspectives

The development of a numerical model is essential for predicting the hygrothermal performance of MBCs across varied climatic conditions and building envelope settings. Given the material's highly porous structure and rapid response to hygric changes, integrating a hysteresis model becomes crucial to account for consecutive wetting and drying cycles and their impact on moisture adsorption and retention. Additionally, incorporating non-isothermal models to couple thermal and hygric boundary conditions enhances the practicality of the model across diverse temperature ranges.

Research would benefit from optimizing fabrication processes to reduce variability in mechanical properties, assessing long-term durability under environmental stressors like humidity and temperature fluctuations, and investigating a wider range of substrates and additives to enhance hygrothermal and structural performance. Testing these composites in full-scale building systems and conducting detailed life-cycle assessments to quantify environmental benefits could further support their practical adoption as sustainable insulation materials.

Author Contributions: Conceptualization, S.M., D.R.R. and G.P.; methodology, S.M., D.R.R. and G.P.; validation, S.M., D.R.R. and G.P.; formal analysis, S.M.; investigation, S.M.; resources, D.R.R.; data curation, S.M.; writing—original draft preparation, S.M.; writing—review and editing, S.M., D.R.R. and G.P.; visualization, S.M.; supervision, D.R.R. and G.P.; project administration, D.R.R. and G.P. All authors have read and agreed to the published version of the manuscript.

Funding: This research received no external funding.

Data Availability Statement: The original contributions presented in this study are included in the article. Further inquiries can be directed to the corresponding author.

Acknowledgments: We gratefully acknowledge Arash Jamali from the Plateforme de Microscopie Électronique at Université de Picardie Jules Verne (UPJV), and Rose Marie Dheilly from the Laboratoire des Technologies Innovantes (LTI), UPJV, for their valuable assistance and expertise in acquiring and analyzing the SEM images used in this study.

Conflicts of Interest: The authors declare no conflict of interest.

Nomenclature

Symbols:

A_c	Absorption coefficient of water [$kg \cdot m^2 \cdot s^{-1/2}$]
β	Volumetric shrinkage percentage [%]
$D_{l,w}$	Liquid diffusivity [$m^2 \cdot s^{-1}$]

$D_{v,w}$	Vapor diffusion coefficient [$m^2 \cdot s^{-1}$]
$D_{v,\varphi}$	Linear dichroism [$kg \cdot m^{-1} \cdot s^{-1}$]
D_{ws}	Capillary suction transport coefficient [$kg \cdot m^2 \cdot s^{-1/2}$]
d	Thickness of the specimen [m]
F	Applied force [N]
g_v	Vapor flux [$kg \cdot m^{-2} \cdot s^{-1}$]
g_w	Liquid flux [$kg \cdot m^{-2} \cdot s^{-1}$]
k	Thermal conductivity [$W \cdot m^{-1} \cdot K^{-1}$]
L	Sample length [m]
n	Porosity of the material [-]
P_v	Water vapor pressure [Pa]
$P_{v,sat}$	Saturation vapor pressure [Pa]
RH_{max}	Maximum relative humidity level [%]
RH_{min}	Minimum relative humidity level [%]
S	Surface area exposed to moisture exchange [m^2]
σ	Flexural strength [MPa]
T	Temperature [K]
u	Moisture content [$kg \cdot kg^{-1}$]
V_f	Final volume [m^3]
V_i	Initial volume [m^3]
w_f	Free water saturation [$kg \cdot m^{-3}$]
Greek Characters:	
δ	Water vapor permeability in air [$kg \cdot m^{-1} \cdot s^{-1} \cdot Pa^{-1}$]
δ_p	Water vapor permeability [$kg \cdot m^{-1} \cdot s^{-1} \cdot Pa^{-1}$]
μ	Water vapor diffusion resistance factor [-]
μ^*	Water vapor diffusion resistance factor in dry condition (50–93% RH) [-]
ϕ	Relative humidity [%]
ξ_ϕ	Slope of the sorption isotherm [$kg \cdot m^{-3}$]
ρ_0	Dry density of the material [$kg \cdot m^{-3}$]
ρ_w	Density of water at 23 °C [$kg \cdot m^{-3}$]
Abbreviations:	
DVS	Dynamic Vapor Sorption
GHOP	*Ganoderma lucidum*, Hemp, Without additive, Pasteurized
GHOS	*Ganoderma lucidum*, Hemp, Without additive, Sterilized
GHOU	*Ganoderma lucidum*, Hemp, Without additive, Unpasteurized
GHWU	*Ganoderma lucidum*, Hemp, With additive, Unpasteurized
GHWS	*Ganoderma lucidum*, Hemp, With additive, Sterilized
GSOS	*Ganoderma lucidum*, Straw, Without additive, Sterilized
GSWP	*Ganoderma lucidum*, Straw, With additive, Pasteurized
GSWS	*Ganoderma lucidum*, Straw, With additive, Sterilized
MBC	Mycelium-Based Composites
MBV	Moisture Buffer Value
TPS	Transient Plane Source
VHOP	*Trametes versicolor*, Hemp, Without additive, Pasteurized
VHOS	*Trametes versicolor*, Hemp, Without additive, Sterilized
VSOP	*Trametes versicolor*, Straw, Without additive, Pasteurized

References

1. Hamilton, I.; Rapf, O.; Kockat, D.J.; Zuhaib, D.S.; Abergel, T.; Oppermann, M.; Otto, M.; Loran, S.; Fagotto, I.; Steurer, N. *Global Status Report for Buildings and Construction*; United Nations Environmental Programme: Nairobi, Kenya, 2020.
2. Jones, D.; Brischke, C. *Performance of Bio-Based Building Materials*; Woodhead Publishing: Sawston, UK, 2017.
3. Beccali, M.; Cellura, M.; Fontana, M.; Longo, S.; Mistretta, M. Energy retrofit of a single-family house: Life cycle net energy saving and environmental benefits. *Renew. Sustain. Energy Rev.* **2013**, *27*, 283–293. [CrossRef]

4. Lawrence, M. Reducing the environmental impact of construction by using renewable materials. *J. Renew. Mater.* **2015**, *3*, 163–174. [CrossRef]
5. Cuéllar-Franca, R.M.; Azapagic, A. Environmental impacts of the UK residential sector: Life cycle assessment of houses. *Build. Environ.* **2012**, *54*, 86–99. [CrossRef]
6. Dutil, Y.; Rousse, D.; Quesada, G. Sustainable buildings: An ever evolving target. *Sustainability* **2011**, *3*, 443–464. [CrossRef]
7. Cerimi, K.; Akkaya, K.C.; Pohl, C.; Schmidt, B.; Neubauer, P. Fungi as source for new bio-based materials: A patent review. *Fungal Biol. Biotechnol.* **2019**, *6*, 17. [CrossRef]
8. Alaux, N.; Vašatko, H.; Maierhofer, D.; Saade, M.R.M.; Stavric, M.; Passer, A. Environmental potential of fungal insulation: A prospective life cycle assessment of mycelium-based composites. *Int. J. Life Cycle Assess.* **2023**, *29*, 255–272. [CrossRef]
9. Livne, A.; Wösten, H.A.B.; Pearlmutter, D.; Gal, E. Fungal Mycelium Bio-Composite Acts as a CO2-Sink Building Material with Low Embodied Energy. *ACS Sustain. Chem. Eng.* **2022**, *10*, 12099–12106. [CrossRef]
10. Elsacker, E.; Søndergaard, A.; Van Wylick, A.; Peeters, E.; De Laet, L. Growing living and multifunctional mycelium composites for large-scale formwork applications using robotic abrasive wire-cutting. *Constr. Build. Mater.* **2021**, *283*, 122732. [CrossRef]
11. Koh, C.H.; Gauvin, F.; Schollbach, K.; Brouwers, H. Investigation of material characteristics and hygrothermal performances of different bio-based insulation composites. *Constr. Build. Mater.* **2022**, *346*, 128440. [CrossRef]
12. Yang, L.; Park, D.; Qin, Z. Material function of mycelium-based bio-composite: A review. *Front. Mater.* **2021**, *8*, 737377. [CrossRef]
13. Gauvin, F.; Tsao, V.; Vette, J.; Brouwers, H.J.H. Physical properties and hygrothermal behavior of mycelium-based composites as foam-like wall insulation material. *Constr. Technol. Archit.* **2022**, *1*, 643–651.
14. Schultz, N.; Fazli, A.; Piros, S.; Barranco-Origel, Y.; DeLa Cruz, P.; Schneider, D.Y. Characterization of Mycelium Biocomposites under Simulated Weathering Conditions. *ACS Appl. Bio Mater.* **2024**, *7*, 8408–8422. [CrossRef]
15. Farrahnoor, A.; Sazali, N.A.A.; Yusoff, H.; Zhou, B.T. Effect of beeswax and coconut oil as natural coating agents on morphological, degradation behaviour, and water barrier properties of mycelium-based composite in modified controlled environment. *Prog. Org. Coat.* **2024**, *196*, 108763. [CrossRef]
16. Stelzer, L.; Hoberg, F.; Bach, V.; Schmidt, B.; Pfeiffer, S.; Meyer, V.; Finkbeiner, M. Life cycle assessment of fungal-based composite bricks. *Sustainability* **2021**, *13*, 11573. [CrossRef]
17. Haneef, M.; Ceseracciu, L.; Canale, C.; Bayer, I.S.; Heredia-Guerrero, J.A.; Athanassiou, A. Advanced materials from fungal mycelium: Fabrication and tuning of physical properties. *Sci. Rep.* **2017**, *7*, 41292. [CrossRef]
18. Elsacker, E.; Vandelook, S.; Brancart, J.; Peeters, E.; De Laet, L. Mechanical, physical and chemical characterisation of mycelium-based composites with different types of lignocellulosic substrates. *PLoS ONE* **2019**, *14*, e0213954. [CrossRef] [PubMed]
19. Künzel, H. *Simultaneous Heat and Moisture Transport in Building Components: One- and Two-Dimensional Calculation Using Simple Parameters*; Fraunhofer IRB Verlag: Stuttgart, Germany, 1995; 65p.
20. Promis, G.; Douzane, O.; Le, A.T.; Langlet, T. Moisture hysteresis influence on mass transfer through bio-based building materials in dynamic state. *Energy Build.* **2018**, *166*, 450–459. [CrossRef]
21. Cai, J.; Han, J.; Ge, F.; Lin, Y.; Pan, J.; Ren, A. Development of impact-resistant mycelium-based composites (MBCs) with agricultural waste straws. *Constr. Build. Mater.* **2023**, *389*, 131730. [CrossRef]
22. Adaskaveg, J.E.; Gilbertson, R.L. In vitro decay studies of selective delignification and simultaneous decay by the white rot fungi *Ganoderma lucidum* and G. tsugae. *Can. J. Bot.* **1986**, *64*, 1611–1619. [CrossRef]
23. Gaff, M.; Hosseini, S.B.; Paulasová, D.; Kamboj, G.; Rezaei, F.; Paul, D. Functionality of production processes in mycelium-based composites. *Compos. Struct.* **2024**, *344*, 118309. [CrossRef]
24. Rahim, M.; Douzane, O.; Le, A.T.; Promis, G.; Langlet, T. Characterization and comparison of hygric properties of rape straw concrete and hemp concrete. *Constr. Build. Mater.* **2016**, *102*, 679–687. [CrossRef]
25. Jiang, J.; Zhou, P.; Yi, Y.; Chen, D.; Hu, G.; Liu, X.; Tang, L. Dual-crosslinked network structured polybenzoxazine/PBO nanofiber aerogel with thermal insulation, flame retardancy, and super-hydrophobicity. *Polym. Degrad. Stab.* **2025**, *234*, 111216. [CrossRef]